Available online at www.sciencedirect.com
ScienceDirect
Comput. Methods Appl. Mech. Engrg. 365 (2020) 112961
Computer methods in applied mechanics and engineering
www.elsevier.com/locate/cma

Level set splitting in DEM for modeling breakage mechanics

John M. Harmon[a], Daniel Arthur[a], José E. Andrade[a,*]

[a] *California Institute of Technology, United States of America*

Received 19 August 2019; received in revised form 20 February 2020; accepted 22 February 2020
Available online 25 March 2020

Abstract

Brittle breakage of particles in granular materials has often been modeled using the discrete element method (DEM). DEM is often limited however in its ability to capture particle shape, particularly when used for breakage. This paper presents the first brittle breakage technique where level set functions will allow for the description of arbitrary shape for both particles and fracture surfaces. The breakage model to be described here uses fracture surfaces defined by level sets to take advantage of simple intersection and difference set operations to split particles in both two and three dimensions. We show how this method is implemented and how we can use it to define and apply arbitrary fracture surface shapes. We then give qualitative examples of using the method in both simple and exotic ways. Finally, we model oedometric tests and rock crushing, both very common uses for previous DEM breakage techniques, to present a validation that the method captures the physics of the problem.

Keywords: Breakage; DEM; Level Set; Geomechanics

1. Introduction

Understanding the mechanics and effects of particle breakage is important in many applications. In geomechanics, particle breakage produces a new particle size distribution (PSD) which will affect strength and dilantancy among other properties [1,2]. Fault zones in earthquakes are home to a large amount of fractured rocks in which the PSD has large effects on the physical attributes on the fault core [3]. Recent continuum models will include breakage as a parameter, which opens the possibility of bridging the grain scale and continuum scale if a grain scale method can reasonably simulate enough grains [4]. Also instead of looking at how particle breakage affects larger scales, one could also look at how a single particle fully comminutes. This has applications in mining, where crushing iron ore is necessary in the process to extract iron [5]. This also has applications in lithotripsy, where the goal is to comminute a single kidney stone as much as possible [6].

Discrete Element Modeling (DEM) has been a popular numerical method for studying breakage. DEM is a method first developed by Cundall & Strack [7] which has been widely used to study granular materials. Implementing particle breakage in the classical DEM, where each particle is a sphere, has been done in two ways. The first is by having each particle made of many smaller particles bonded together [8–12]. When the forces acting between two smaller particles exceed the strength of the bond, then the bond is considered fractured and therefore

* Corresponding author.
E-mail address: jandrade@caltech.edu (J.E. Andrade).

https://doi.org/10.1016/j.cma.2020.112961

removed. The benefits of this method are that an initial clump of particles can be arranged to take a non-spherical shape and the fracture will preserve mass. The drawbacks are that the increased amount of particles increases computation time and even with an extremely large amount of smaller particles, the larger particle will always differ from a physical one. The other method replaces a particle when it reaches a certain stress level with many smaller particles [13,14]. This method is much quicker computationally, but has issues with mass conservation, replicating a realistic fracture pattern, and choosing how many particles to replace a larger one with.

Both the sphere-based methods mainly suffer from an inability to model particle shape correctly, which in recent literature has shown to have an impact on which grains carry the deviatoric stresses [15]. Since it is the stresses on the particle that drive when and how particles break, it is critical to have a method that describes particle shape exactly.

This has been approached by creating and solving a finite element mesh for every particle [16,17], a good solution for granular systems with small numbers of particles. For larger systems, polyhedral elements have been used. Originally done by Potapov and Campbell [18], this was originally quite slow so this method was modified to be suitable for large scale simulations [19]. The improved method has not been able to fit both single particle breakage and particle size distributions though due to an energy based approach instead of a stress based one [20]. More recent developments have moved to a stress based approach and increased efficiency using ideas such as implementing a hybrid peridynamcis and physics engine approach [21]. Despite these advancements, polyhedral methods still have difficulty working with geometrical concavity in particles. Since it should always be expected that particles will have local concave features, these methods are not fully ideal.

A version of DEM that can handle non-convex particles uses Fourier descriptors to describe shape [22]. Fourier descriptors can effectively describe any particle of a "star" shape, which is suitable for most granular materials. As far as we have seen, there is no breakage method for this DEM version yet.

In this paper we will build a breakage model from the level set DEM (LS-DEM) [23]. This method has the powerful capability to capture exact shape without limitations while maintaining reasonable computational efficiency. LS-DEM has the profound advantage of capturing morphology from X-ray Computed Tomography (XRCT) [24] and has been shown to be able to make one-to-one predictions at the micro-scale [25]. So in the following sections we will describe the first LS-DEM breakage method. We will first show how splitting level sets can be done in both two and three dimensions. Then we will show an industrial example of how level set splitting in LS-DEM can predict the performance of crushing machines. Finally, we will show an example of the method's capability in geomechanics from comparisons with oedometric experiments on a granular specimen, with a small study of breakage criteria.

2. LS-DEM

LS-DEM, originally introduced in [23], is a DEM variant that fully captures the shape of every particle unlike the classical DEM where only spheres are used. LS-DEM utilizes level set functions for defining each particle geometry. Level set functions define a surface implicitly by having the function value at every point be equal to the signed distance to the object surface; a negative level set value means the point is inside the object, a positive value for outside the object and a zero value for locations on the surface.

In implementation, particles of dimension D are geometrically defined by using both a discrete level set, ϕ,

$$\phi(\mathbf{x}) = \pm d \tag{1}$$

where d is the signed distance from the surface of the particle and a set of surface points, P,

$$P = \{\mathbf{p} \in \mathbb{R}^D | \phi(\mathbf{p}) = 0\} \tag{2}$$

as shown in Fig. 1. This method of contact results in efficiency being largely based on surface point discretization density since each point must be checked with either the level set of each other particle or the radius of its bounding sphere. The discretization of the level set has no effect on efficiency outside of a finer grid taking more memory to store.

To find contact, for instance between particle g_1 and particle g_2, we take the surface points of g_1 and check the level set value on g_2 of each surface point. If the following inequality holds for any surface point, $\mathbf{p}_i \in P_1$, on the first particle,

$$\phi_2(\mathbf{p}_i) < 0 \tag{3}$$

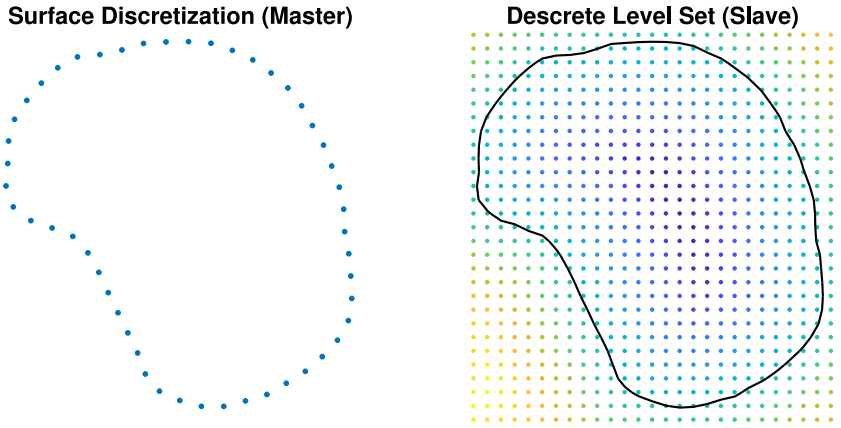

Fig. 1. Left: A set of points that all lie on the particle surface. Right: A discrete color map where cooler colors are negative and warmer colors are positive. The black line is the zero contour line found with interpolation. The surface points of the master particle are mapped to the slave particle's level set to determine contact.

then contact is established and the overlap is known from the evaluation of $\phi_2(\mathbf{p}_i)$. Furthermore, the contact normal is calculated easily from the gradient of the level set,

$$\hat{\mathbf{n}} = \nabla\phi_2(\mathbf{p}_i) \tag{4}$$

With the overlap and contact normal, contact forces and moments can be determined from a contact law. No contact law is specific to LS-DEM; in this study a linear model is used. The Hertzian contact law could also be used [26]. The frictional forces are computed using Coulomb friction. These forces and moments are then integrated to get displacements and rotations for each time step. Either contact dynamics [27] or an explicit scheme [28,29] could be used for integration, and in this paper the explicit scheme is chosen. The displacements and rotations are then applied to the surfaces points and the process iterates.

3. Description of breakage model

The breakage model described here is composed of two parts. The first part is the fracture criterion, which determines when a particle will break. This part is not specific to the method and can easily be changed as will be discussed. The second part is the level set splitting method, which determines how a particle will break. This method was built with the assumption that the particles which compose the granular material are brittle. Namely, that the speed of crack propagation is on a much smaller time scale than the loading. With this assumption in mind, it is sensible to build a method that breaks a particle into two or more pieces instantly, or in implementation, a single time step. This can save a significant amount of computation time that would otherwise be used for crack tracking, determining crack speed or resolving stress around a crack tip allowing a user to model systems with very large numbers of breakages.

3.1. Breakage criterion

A natural way to determine when a particle should break is by evaluating the stress inside the particle. This can be done by solving the distribution of stresses in a particle [16] however this method can be very inefficient. Alternatively, the average stress inside the particle, $\bar{\boldsymbol{\sigma}}^p$ can be calculated from knowledge of the contact forces, $\mathbf{F}_c$, and branch vectors, $\mathbf{x}_c$, over a certain number of contacts on the particle, N,

$$\bar{\boldsymbol{\sigma}}^p = \frac{1}{V_p}\sum_{c=1}^{N} \boldsymbol{x}_c \otimes \boldsymbol{F}_c \tag{5}$$

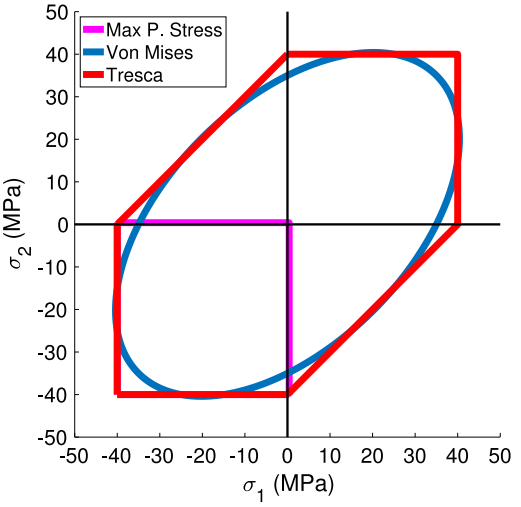

Fig. 2. Yield surfaces used in this paper.

where V_p is the volume of the particle. From here it is very convenient to find the principal stresses, σ_p by finding the eigenvalues of $\bar{\boldsymbol{\sigma}}^p$.

$$(\bar{\boldsymbol{\sigma}}^p - \sigma_p \mathbf{I})\hat{\mathbf{n}} = 0 \tag{6}$$

Using the principal stresses we can then choose a stress based yield criterion. As mentioned before, the yield criterion is a flexible choice, therefore in this paper three separate yield criteria will be used. Here we will use the maximum principal stress, von Mises criterion, and the Tresca criterion for breakage however other DEM breakage models have also used a shifted Tresca criterion [17] which could certainly be substituted given considerations for the material being modeled.

The maximum principal stress criterion assumes that the particle will break when the principal stresses reach a critical value. For this criterion, we will assume this could be in either compression or tension. Since most granular materials are much stronger in compression than tension, there will be two critical values for this criterion.

$$\sigma_C^{max} > \sigma_C = min(\sigma_{p1}, \sigma_{p2}, \sigma_{p3}) \tag{7}$$

$$\sigma_T^{max} > \sigma_T = max(\sigma_{p1}, \sigma_{p2}, \sigma_{p3}) \tag{8}$$

where σ_C and σ_T are the maximum compressive and tensile stresses respectively.

The von Mises yield criterion is expressed as follows,

$$\sigma_{Vmax} > \sigma_V = \sqrt{\frac{1}{2}[(\sigma_1 - \sigma_2)^2 + (\sigma_2 - \sigma_3)^2 + (\sigma_3 - \sigma_1)^2]} \tag{9}$$

where σ_{Vmax} is the maximum allowed value of the average von Mises stress inside a particle, σ_V.

The Tresca yield criterion is based on the shear stresses in the material

$$\frac{1}{2}\sigma_C^{max} > \tau = \frac{1}{2}max(|\sigma_1 - \sigma_2|, |\sigma_2 - \sigma_3|, |\sigma_3 - \sigma_1|) \tag{10}$$

where τ is the maximum shear stress at any one stress state. Fig. 2 shows a graphical depiction of the yield surfaces from these criteria. The units are set to be the stress values for the oedometer test in Section 5 of this paper.

When the average critical stress of any particle exceeds the threshold set by the chosen criterion then the particle will be broken. The value of the critical stress is determined by both the material and the size of the particle, as according to Weibull's theory [30] the probability of failure is given by

$$P_f(\sigma^c \geq \sigma^{max}) = 1 - exp\left\{-\left(\frac{d}{d_0}\right)^3 \left(\frac{\sigma^c}{\sigma_0}\right)^m\right\} \tag{11}$$

where d and σ^c are the diameter and the chosen breakage criterion's characteristic stress for any given particle, and d_0 and σ_0 are a reference diameter and strength. The variable m is Weibull's modulus which is a material parameter. In this paper a typical Weibull's modulus of 3 was used throughout [31]. To be able to seed true critical stress values we need to invert and solve for σ^c.

$$\sigma^c = \sigma_0 \left\{ -\left(\frac{d_0}{d}\right)^3 ln(1 - P_f) \right\}^{m^{-1}} \tag{12}$$

Now by using inverse transform sampling, we can seed critical stress values by taking values of P_f from a uniform distribution, $U(0, 1)$.

As particles break into smaller fragments, breakages tend to be along the largest flaws in a given particle. Therefore as particles comminute they will become stronger which is an effect that must represented in modeling. To continue to account for particle size in our breakage criterion, we refer to Weibull statistics and experiments performed by Nakata et al. [32] that show the following relation between a child particle, a, and a parent particle, b,

$$\frac{\sigma_a^{max}}{\sigma_b^{max}} = \left(\frac{d_a}{d_b}\right)^{-3/m} \tag{13}$$

3.2. Level set splitting

Splitting particles in LS-DEM can be done in either two or three dimensions, and have a similar process for each. To split a level set, ϕ_1, we first must make a separate level set object that defines the fracture surface we want to apply, ϕ_2. The fracture level set surface must extend to the boundary at all end points, allowing one side of the surface to have negative values and the other to have positive values. These fracture surface level sets can be made in a wide variety of ways. Some methods of creation could be: level set imaging from XRCT just like grains of sand in previous uses of LS-DEM [24], utilizing stress distribution information that could be solved on the particle [33], or from assumptions on what the fracture might look like based on contact forces and/or particle shape.

The two new grains will be created by doing the intersection and difference set operations between ϕ_1 and ϕ_2.

$$\phi_3 = \phi_1 \setminus \phi_2 = max(\phi_1, -\phi_2) \tag{14}$$

$$\phi_4 = \phi_1 \cap \phi_2 = max(\phi_1, \phi_2) \tag{15}$$

This process is depicted in Fig. 3 for both a 2D and a 3D grain. Note that both surfaces can have large numbers of convexities and concavities and that every feature that intersects the particle is shown in the fragments. The part of fracture surfaces that extend past $\phi_1(\mathbf{x}) = 0$ can be arbitrary.

Since the new particle surfaces defined by ϕ_3 and ϕ_4 are made by set operations, the union operator could also be used to bring back the original particle,

$$\phi_3 \cup \phi_4 = min(\phi_3, \phi_4) = \phi_1 \tag{16}$$

The intersection and difference set operations can produce error on the outside region of each fragments' level set, or specifically where $\phi > 0$. These errors come from the set of kept distance values that refer to a surface that was removed during the set operation. Due to LS-DEM only being interested in the level set values inside the particle, this issue can be safely ignored for most cases. The accuracy of the outer portions could be important if we wanted to add cohesion or a bonding method though. In this case, these errors can be removed with a couple of time steps of the reinitialization equation which was first described in [34],

$$\phi_t = sign(\phi_0)(1 - |\nabla\phi|) \tag{17}$$

The reinitialization equation keeps the object surface stationary and converges when the level set returns to being a signed distance function at all points. After reinitialization the particle is ready for use for all purposes. In Fig. 4 a heat map of the errors is shown for ϕ_1 after being split by a straight line. The error is calculated from the difference in the discrete level set values from the broken particle before and after reinitialization. The dots on the figure depict the discrete border where the set operation stops taking values from the original particle (red dots) and

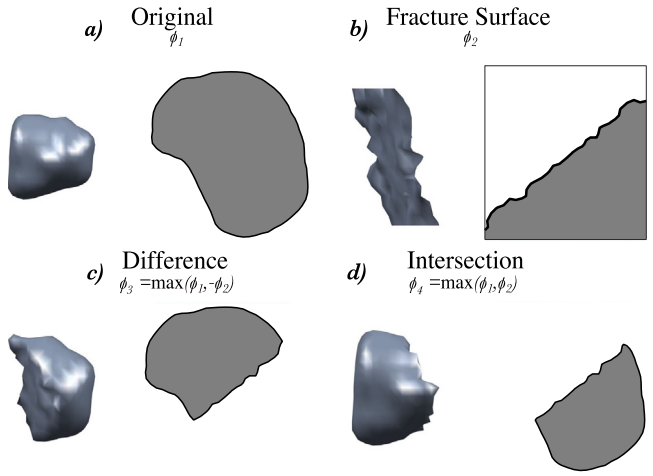

Fig. 3. Level set surfaces in 2D and 3D for a pre-split sand grain (top left), breakage surface (top right), and two fragments (bottom left and right).

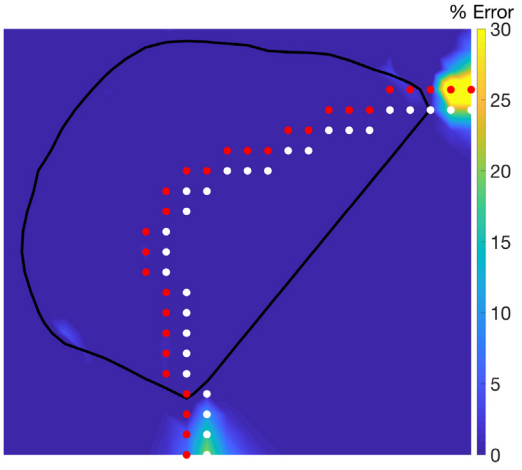

Fig. 4. Heat map of the error produced from set operations. Dots on figure show the discrete border between the max function picking particle values (red) or fracture surface values (white). (For interpretation of the references to color in this figure legend, the reader is referred to the web version of this article.)

starts taking values from the fracture surface (white dots). It can be easily seen that errors are localized to areas outside of the resulting particle. Since no cohesion was necessary for any application in this paper, Eq. (17) is not used.

3.3. Determining fracture path

While it is possible to use any arbitrary fracture surface that could be derived from either experiment or statistical methods, the simplest way to implement level set splitting into LS-DEM and the way it will be done in this paper is to only use flat breakages such as lines in 2D and planes in 3D. These breakages can be oriented in any way by defining the line or plane by two or three points respectively. Experiments have shown that granular fracture surfaces are highly likely to connect between the contact forces acting on a grain [35,36]. So for the case of 2D, we choose the two points to complete the line by taking the location of the two highest contact forces. From here

the level set can be easily built from the well known point to line distance formula,

$$\phi(x, y) = \frac{(y_2 - y_1)x - (x_2 - x_1)y + x_2 y_1 - y_2 x_1}{\sqrt{(y_2 - y_1)^2 + (x_2 - x_1)^2}} \tag{18}$$

where the locations of the contact points are given as (x_1, y_1) and (x_2, y_2).

Similarly in 3D, we choose the locations of the three highest contact forces to determine the breakage plane. With these locations determined from contact, the resulting level sets can be calculated from,

$$\phi(\mathbf{x}) = \frac{\mathbf{n} \cdot \mathbf{x} - \mathbf{n} \cdot \mathbf{p}_1}{\|\mathbf{n}\|} \tag{19}$$

where

$$\mathbf{n} = (\mathbf{p}_2 - \mathbf{p}_1) \times (\mathbf{p}_3 - \mathbf{p}_1) \tag{20}$$

and $\mathbf{p}_1$, $\mathbf{p}_2$, and $\mathbf{p}_3$ are the three points that define the plane. For both two or three dimensions, there are occasionally cases where only one or two forces cause enough stress to break a particle which would not create enough contact points to complete a line or plane. For these cases the particle centroid was used as another point for breakage. In the case that there is only one contact point for a 3D particle, breakage was held off until a second contact point was encountered. If there are multiple points of contact for a single contact pair, such as right after a breakage with line-to-line and plane-to-plane contact, only the point of contact contributing the highest force will be used for fracture path determination.

To build the surface points, generally a marching squares method or an energy minimization method is used. In the case of building flat fracture surfaces this can be greatly simplified by utilizing the known vectors that define the line or plane and placing points at equidistant values along the tangent vector directions. From here, we determine which surface points from the original particle and the fracture surface go to which fragment. This is done by comparing surface points to the level sets. For example, if the locations of surface points on the fracture surface are in the negative region of the original particle's level set, then we keep those points since these will be on the surface of both fragments. Similarly, we check the location of each surface point on the original particle against the fracture path level set to determine which fragment that surface point should be assigned to.

During fragmentation, the physical properties of the new particles must also be determined, namely the mass, moment of inertia and center of mass. This is done using just the level set matrix in the same way as when producing particles from tomography. A full explanation for how to calculate these properties is both in [23] and in the Appendix.

3.4. Qualitative testing

Before applying the model to applications for validation, we first went through a round of qualitative testing. The first of these was producing the breakage of three grains vertically aligned in compression shown in Fig. 5. This was conducted both in 2D and 3D on particles of Hostun sand taken from 3D XRCT. The DEM parameters were set to produce breakages easily in order to test the stability of small particles. It was here that it was found that when particles become small enough to be of similar size to the surface point discretization then they can be a source of significant instability. We had three methods to address this issue. First method is to halt breakage when particles reach a minimum size. The second method is to adaptively increase discretization of the particles throughout comminution. The final method was to remove particles that were small enough to be problematic. All three of these methods were tested in the two quantitative studies described in the following sections. The first method was unable to produce good results against experiment for predicting PSD since the smaller sizes were unreachable by definition. It is likely that this method would be a good one if the particles were given a finer discretization since the limiting factor was often the surface point discretization density. The later two methods both produced similar results so the final method was used throughout due to its added efficiency. Removed particles were stored in output and were counted in producing the PSD data. For all simulations, it was ensured that the total mass of the filtered particles was $< 1\%$ of the total mass of the specimen.

It is also of note that after some qualitative analysis of this method it was found that occasionally a seemingly unrealistic amount of thin grains were produced, particularly in 2D. To remedy this we also added what was termed a "buckling" breakage mode. The buckling mode occurs if the volume of the circumscribed circle or sphere around

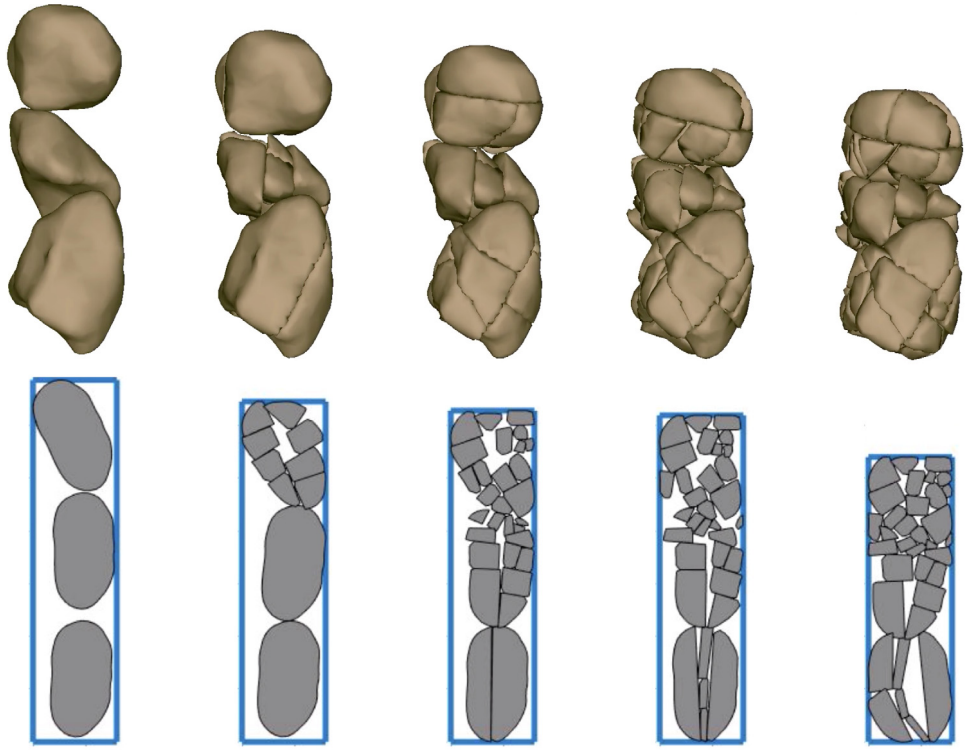

Fig. 5. A simple three particle example for level set splitting for both 3D (top) and 2D (bottom).

the particle is much larger than the volume of the particle itself. If a calibrated ratio between the circumscribed sphere's volume to the particle volume was reached then the particle would be cut along its closest surface. So in this case the breakage line would be determined from the centroid and the closest surface point, p_{min}, from the set of surface points for each particle, P_p,

$$p_{min} = min(P_p) \tag{21}$$

which would define the fracture line in 2D. In 3D we took a random point to complete the plane with the centroid and p_{min}. This was not used in later testing with experiment since it did not produce good results, an explanation for this will be given in Section 5.1. So while this was used during qualitative tests, this was not used in any other part of the paper.

For the next qualitative test, we wanted to look at a more dynamic setting that clearly demonstrates an ability that no other DEM breakage model could produce in a practical way. For this we took the fact that the ability of level sets to take arbitrary shape is a unique and powerful ability within the context of DEM. There are many applications, particularly in breakage mechanics, where extremely complex shapes may need to be used. A good example of this is in building demolition, where both the wall and the demolition machine have shapes that are very different than any granular particle. We take advantage of the geometrical versatility of using a level set based method to show an example of how this method could be used for demolition.

The set up consisted of creating both a wall and excavator buckets in AutoCAD and then converting each into level sets through a point-to-triangulation distance function. The bucket trajectories were then defined so that there would be two instances of crushing the wall. For each instance of wall crushing, the first break was manually determined in order for the breakage method to not choose the centroid of the wall as a point on the breakage plane. All subsequent breakages were done by using the flat level set splitting breakage method described earlier. The final product of this is a video where five representative frames at different phases of the demotion are shown in Fig. 6. This simulation demonstrates that level set splitting in DEM can be used in many applications beyond the typical uses for DEM in granular mechanics.

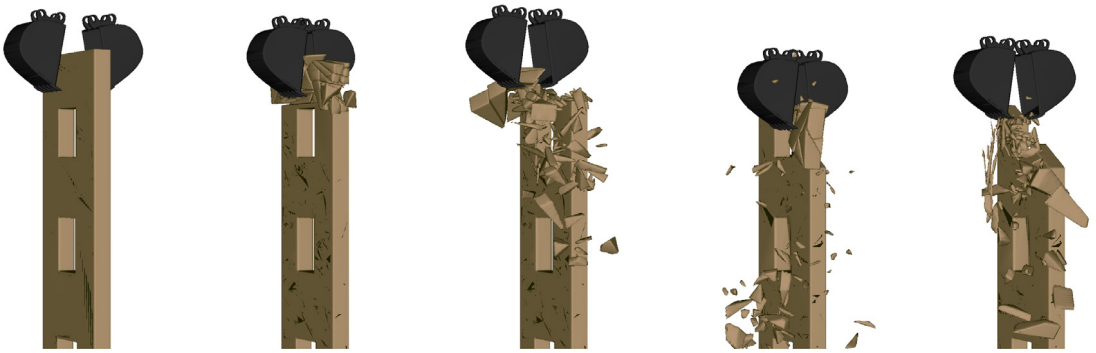

Fig. 6. Visualization of wall demolition using two excavator buckets. Simulation time runs from left to right.

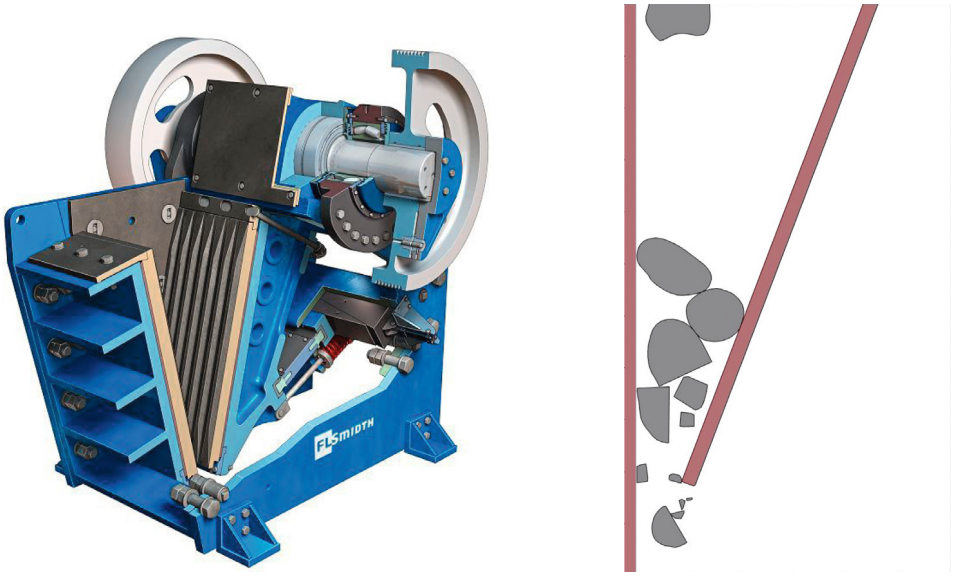

(a) TST Jaw crusher made by FLSmidth.

(b) Visualization of a 2D jaw crusher in operation

Fig. 7. Jaw crushers.

4. Jaw crusher simulations

4.1. Jaw crusher setup

DEM has been a popular method for simulating rock crushing for mining applications [37]. One of the simplest crushers is the jaw crusher which will be used as an example in this section. The jaw crusher uses two plates to comminute rocks by compressing the plates together repeatedly. As shown in Fig. 7a, these plates are either vertical or near vertical and taper to create a much smaller opening at the bottom than at the top. In all jaw crushers there are a stationary plate and a swing plate. The swing plate can be set to have specific opening sizes, RPMs, and other adjustable settings depending on how it is manufactured.

The jaw crusher simulations were built to mimic the jaw crusher used in a study by Johansson et al. [38]. The table below shows the three crusher specific settings that we looked to mimic. The first is the rotational speed of the wheel that drives the compression of the plates. One rotation of the wheel corresponds to one cycle of compression and extension. The second is the average angle between the stationary plate and swing plate which is called the nip angle. The swing plate will tilt slightly during operation. In our simulations the angle varied $\approx \pm 1.7$ degrees

Table 1
Parameters for jaw crusher testing.

Parameter	Value	Units	Jaw crusher setting	Value	Units
k_n	$3 * 10^7$	N/m	RPM	300	rotations/min
k_s	$0.8 * k_n$	N/m	Nip angle	22	degrees
μ	0.6	None	Nip angle variation	$\pm$ 1.7	degrees
ρ	2650	kg/m^3	Eccentric throw	50	mm
Δt	$1.8 * 10^{-6}$	s	k_n	$3*10^7$	N/m
Global damping (C_g)	0	$(s)^{-1}$	k_s	$0.8 * k_n$	N/m
Contact damping (C_{res})	0.4	None	μ	0.6	None
Level set resolution	7	mm/pix			
Weibull's modulus (m)	3	None			
Critical strength	56.5	MPa			
Characteristic diameter	0.21	m			
Surface point discretization density	2	pts/pix			

each rotation. The third is the eccentric throw, which is the distance between the open side setting (OSS) and the closed side setting (CSS). The OSS being the widest opening between the bottom of the plates and the CSS being the smallest opening over a cycle.

This jaw crusher simulation will be done in 2D with two rectangles defined by level sets representing the jaw crusher. The rock shapes used were cross sections of Hostun sand from XRCT images scaled to the size of rock. A total of 25 unique particle shapes were used and dropped in order so that the twenty-sixth particle that was dropped was the same as the first particle. The feed for the jaw crusher was done by dropping rocks into the crusher from a specified position once the last rock had completely cleared the space. Fig. 7b shows a visualization of the jaw crusher during a simulation. The particle on the upper left shows where the particles are spawned, and particles were sent to output once they left the frame of the image. Simulation parameters were set to resemble typical values for rock and shown in Table 1. For these simulations only the von Mises criterion was used. Studying the effect of using this criterion versus the Tresca and Maximum Principal Stress will be done in the next section on oedometer testing.

4.2. Jaw crusher results

There were three total simulations analyzed for comparison. The closed side setting (CSS) was varied from 50 mm, to 80 mm and then to 100 mm while all other parameters, including calibrated material parameters, were kept constant. Each simulation was run over forty jaw crusher cycles. The total amount of particles analyzed as output was 336, 397, and 233 for the 50 mm, 80 mm and the 100 mm CSS test respectively. At the end of each simulation, the PSD was determined for the collection of particles that had completely passed through the crusher. Sieve size was determined through an approximation of the minor axis of the particle. We calculated this by finding the diameter along the line connecting the centroid and the closest surface point, p_{min}, from Eq. (21). We then took manufacturer results for output PSD given in [38] and compared them to our simulation in Fig. 8. Results match well for all three comparisons across sieve sizes, which means this modeling strategy can be predictive for applications where output PSD is a key factor.

Although not done here, other important predictions for jaw crushers can be performed using this strategy such as capacity, flow rate, power draw, and effects of different jaw crusher settings. Other crushers besides the jaw crusher could also be modeled easily since level sets can be built from the CAD models used to design crushers.

5. Oedometric testing

Oedometer tests have been a common way to investigate the effect of crushing in a granular sample [39]. These tests are conducted by compressing the specimen from the top, usually in displacement control, while maintaining rigid walls around the specimen. Due to the rigidity of the boundaries, the specimen must have breakages to better fill the constantly decreasing void space. And so to further validate our model quantitatively, we conducted an oedometric test on a set of grains in 2D and compared the results to experimental testing in the literature.

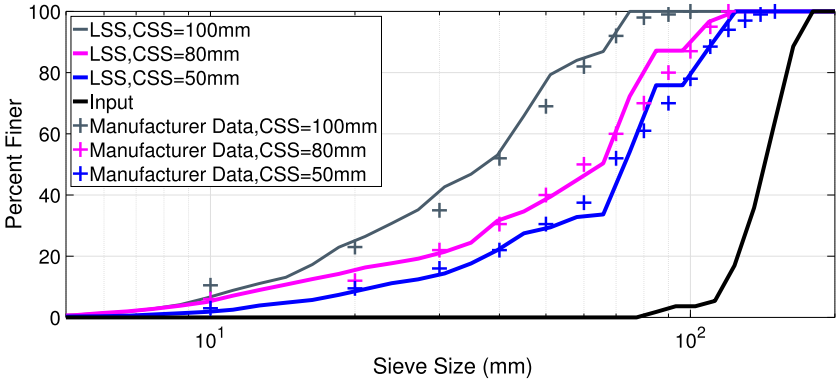

Fig. 8. PSD of the jaw crusher output from both the level set splitting method as well as from experiment. *Source:* Manufacturer data adapted from [38].

Table 2
Parameters for Oedometric testing.

Parameter	Value	Units	Parameter	Value	Units
k_n	$4 * 10^7$	N/m	Weibull's modulus (m)	3	None
k_s	$0.6 * k_n$	N/m	Max compressive stress	40	MPa
μ	0.4	None	Max tensile stress	0.4	MPa
ρ	2450	kg/m^3	Max von mises stress	35	MPa
Δt	$2.2 * 10^{-7}$	s	Max shear stress	40	MPa
Global damping (C_g)	$0.01/\Delta t$	(s)$^{-1}$	Minimum area	0.05	mm^2
Contact damping (C_{res})	0.4	None	Characteristic diameter (d_c)	2	mm
Level set resolution	0.07	mm/pix	Wall strain rate	0.08	mm/s
Surface point discretization density	2	pts/pix			

5.1. Specimen setup

The specimen setup described in this section is intended to simulate a cross section of a cylindrical oedometer test specimen. The grains that were utilized for this were the same shapes as from the crushing example and again were picked from a pool of 25 total grains. The material properties were set the same as the silica sand from oedometric experiments done by Nakata et al. [40] in an attempt to compare our simulation to their experimental results and are shown in Table 2. This was done by calibrating the stiffness so the simulation matches the experiment constitutively in the regime where there is no breakage. The yield stress for the particles was then set so grains would start breaking at the same time as when breakage initiated in the experiment. This resulted in slightly different critical stress values for each criterion. The graphical depiction of these values was presented in Section 3.1 in Fig. 2 and a discussion on this will be left to the next section.

There was no consideration for particular particle shape properties since the actual shapes from the experiment are not known, therefore the accuracy of these tests will be more focused on the physics rather than a one-to-one matching that has been done in previous studies with LSDEM [25]. The initial PSDs were nearly uniform between 1.4 and 1.7 mm for both the simulation and experiment as shown in Fig. 13. Matching the initial PSD is critical since it has been shown in experiment a more graded sample will affect both constitutive properties and final PSD [32,40]. As discussed earlier, initially there was a consideration to have a buckling breakage mode to avoid unnaturally thin particles. While this mode seems intuitive, in application it causes an un-physical kinking in the PSD. We believe this is due to the particles that reach this criterion are set to cut in half, eliminating certain particle sizes from being achievable. An example of this phenomenon is shown in Fig. 9.

The numerical specimen was set to have the same height (10 mm), as the experiment and set to have the same width as the diameter of the experiment (50 mm). Porosity was matched by using an equation suggested by [41],

$$\phi_{2D} = 0.42 * \phi_{3D}^2 + 0.25 * \phi_{3D} \tag{22}$$

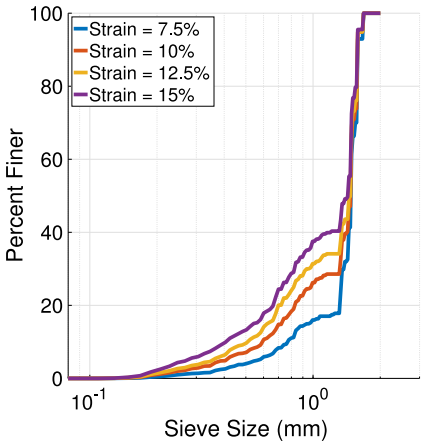

Fig. 9. PSD using the von Mises criterion and the buckling breakage mode. Kinking in the curve can be observed due to the inability of the buckling breakage to achieve a wide range of breakage sizes.

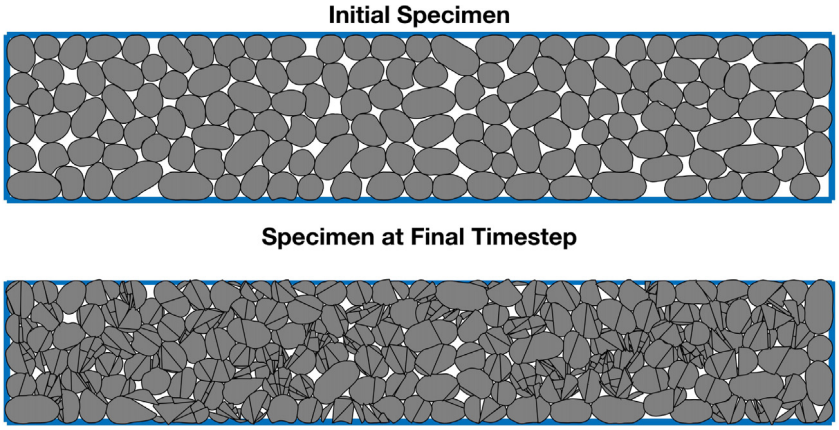

Fig. 10. Visualization of the oedometric test at the initial and final time steps.

which resulted in our simulation having an initial void ratio of 0.18 which corresponds to a three dimensional void ratio of 0.6. With a fixed specimen dimension, the PSD and void ratio targets were achieved by placing in grains that were scaled to match the PSD requirement until the allowable volume of solids in the specimen was reached. This resulted in the final specimen having 144 grains before loading (see Fig. 10).

5.2. Results

The results discussed here are from a set of DEM simulations from the specimen described before. While intended to completely mimic the experiment, only half of the total imposed displacement from experiment was done in simulation. This is because of limits in void space in two dimensions so that the simulation could only reach strains of around 15%. Despite this, many useful comparisons can be made at these lower strain levels.

The results for the model and its comparison to experiment will first be looked at for the constitutive relation. Fig. 11 plots the stress vs strain and void ratio for both the model and experiment. Since LS-DEM without breakage has been validated in previous papers, matching the first three data points was expected as little or no breakage had occurred yet. The comparisons for the breakage model start at around a strain of 5% where the model and data still align quite closely. Some lack of smoothness can be observed during the breakage region for the model which we believe would be greatly minimized from having a larger sample so that individual breakages do not affect the macroscopic properties as heavily. We also observe that all three breakage criteria can achieve the same

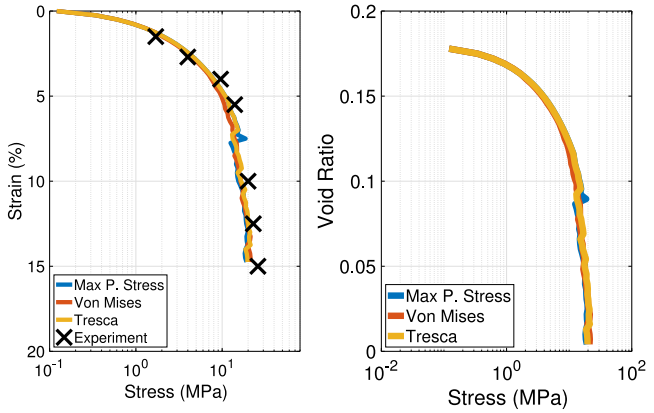

Fig. 11. Stress curves for each stress criterion calibrated to experiment.

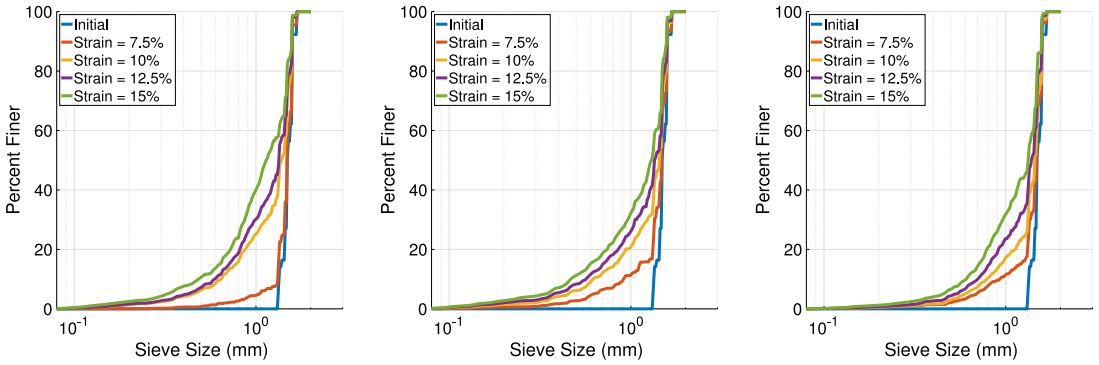

(a) Principal Stress Criterion **(b)** von Mises Criterion **(c)** Tresca Criterion

Fig. 12. Growth of PSD for each criterion studied.

macroscopic response, the main difference being that they must be calibrated to a different value. While the Tresca and maximum principal stress criteria correspond to a compression strength of 40 MPa, the von Mises correspond to a compression strength of 35 MPa. The fact that the Tresca and maximum principal stress criteria predict higher breakage stresses is expected since these are more conservative criterion measures. Considering the very similar constitutive response and the shape of the three yield surfaces, it seems that the most important part of the yield surfaces are the compressive regions where all three yield surfaces overlap.

The PSD was also compared at both the initial and final stages of the test and shown in Fig. 13. Again each criterion produces very similar results and matches closely with experiment. In Fig. 12 the evolution of the PSD is shown showing similar results across all three criteria at high strains. Some differences can be seen for the principal stress criterion at low strain rates, which is likely due to each simulation having a different seed for initial strength values. Once more breakage has occurred, the curves more closely align showing that the true strength distribution is seen by the material response.

While the level of breakage seems to be consistent with experiment, the model predicts slightly more large particles and slightly less small particles. These limitations would likely come from either using only straight cracks on a small specimen or differences in definition of sieve size between two and three dimensional granular materials. Investigating this effect on larger specimens in three dimensions may eliminate this issue, where there would be less statistical variance and the sieve size would be better identified as the three dimensional intermediate axis length instead of the two dimensional minor axis length. Another way that this could be improved is by defining fracture surfaces with more data-intensive methods such as either intra-particle stress distribution methods such as the boundary element method [33] and the ghost-point finite difference methods [42] or from XRCT images of breakage.

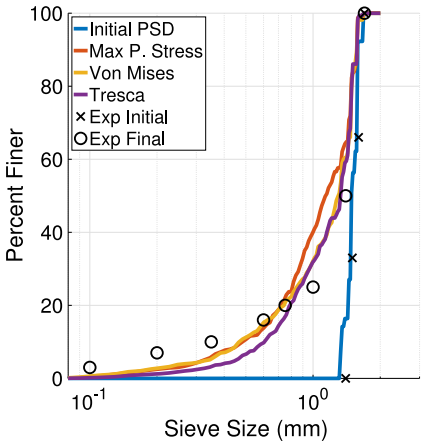

Fig. 13. Particle size distributions at the initial and final states for experiment and simulation using each of the three breakage criteria.

Another interesting trend was found by taking a closer look at the grain scale. Since the level set splitting method can capture exact shape, it is an ideal model for investigating changes in grain shape which we will do for the von Mises criterion simulation. Here we will look at the development of shape by looking at the true circularity, the two dimensional analog to true sphericity, and the aspect ratio (AR) for each particle. The true circularity is measured as the ratio between the circumference of a circle with the particles volume and the perimeter, ρ, of the particle. The calculation for which can be simplified to,

$$Circularity = \frac{4\pi V_p}{\rho^2} \tag{23}$$

For comparison, true sphericity of a particle is defined as the ratio between the surface area of a sphere with the same volume and the surface area [43]. AR here is defined by the ratio between the short axis and the long axis of a best fit ellipse on the particle.

Fig. 14 shows the trend of the average circularity and average AR as a function of the macroscopic vertical strain applied to the specimen. Both true circularity and AR drop as particle sizes get smaller. This is consistent with trends of both AR [44–48], and sphericity [46,47] in experiments. Some experiments however have reported that sphericity can increase during light breakage before sphericity drops during heavy breakage [44]. We believe this is not seen in our results for two reasons. First is that our particles are already very circular at the beginning of the test, so an increase in sphericity would be difficult. The second reason is that this model as of now does not attempt to replicate chipping, which has been experimentally shown to be the dominant breakage phenomenon at lower stress levels, while splitting is dominant at high stress levels [49]. Chipping is the effect of very small breakages focused around a single contact point on a particle. Chipping would likely have a large chance for shaving off sharp corners that would contribute to an initial particle's lack of sphericity, thereby increasing the sphericity after breakage. While chipping is a possible effect to model using level set splitting assuming a certain chipping criterion, it was not attempted in this paper.

Fig. 15 shows a series of particle sphericity and AR histograms as a function of global strain on the specimen. Bins for the histograms were segmented at 0.5 intervals in a way so that the center of the bins is depicted as dots on the figure. Since only 25 unique particles are used, the initial distribution of particle shapes is not well varied. Over the course of the experiment, the particles' circularities and ARs become much more varied. This is to be expected since some particles will break much more than others and cause the particle shapes to take a more varied distribution. These results further suggest that the particle shape has a significant effect on both the likelihood of breakage on any single particle and on the nature of breakage as damage increases.

6. Conclusion

Modeling breakage in granular materials has always been challenging due to the complexities of the breakage process and capturing arbitrary shape changes. This paper presented a modeling method that provides an avenue

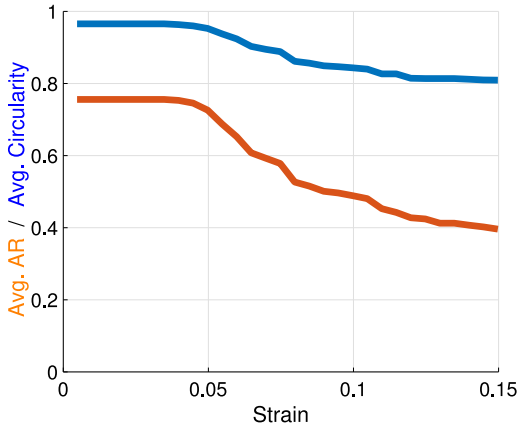

Fig. 14. Trend in average circularity and average aspect ratio of the particles as the macroscopic strain increased on the specimen.

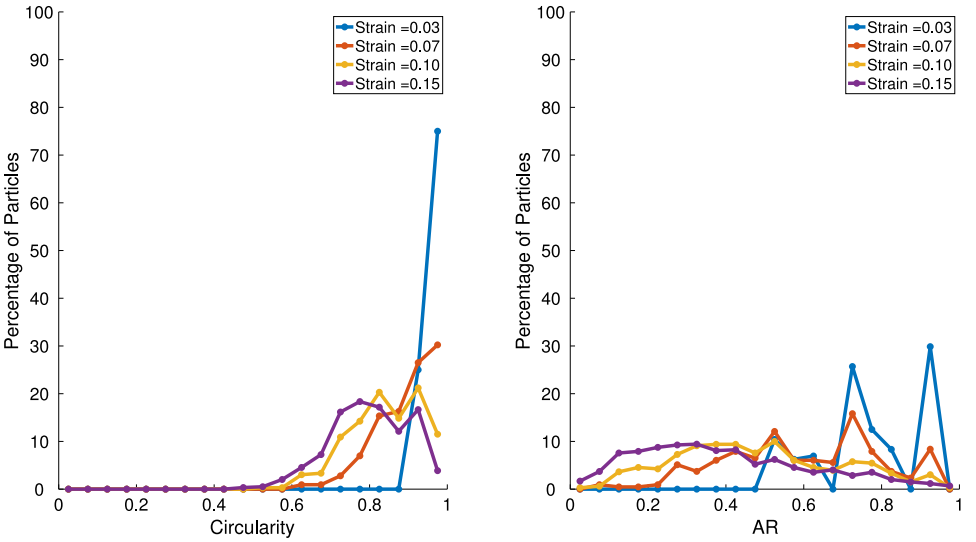

Fig. 15. Histograms of particle circularity and aspect ratio as a function of strain on the specimen.

for addressing the difficulties in modeling the morphological changes that occur in breakage. In doing so, we demonstrated how the level set splitting method can thrive in various realms where DEM finds a use.

The first example was for comminution modeling for a jaw crusher. We showed how the level set splitting method can make very accurate predictions on the PSD of the jaw crusher output. Abilities for this model to make additional important predictions on performance for both jaw crushers and other crusher types were discussed as possible future work. The second example was a classic oedometric test where we showed that level set splitting can make reasonable comparisons with experiment even with quite small samples. In fact predictions could be made at both the macroscopic scale, such as for constitutive modeling, and also at the grain scale, such as with predicting changes in particle shape.

Future work with this method will certainly include quantitative validation exercises in three dimensions, using XRCT to capture the true particle shapes of the material. Further work can also be done with using XRCT to determine the exact time and fracture surface of a breakage, allowing for the study of single particle breaks. This could answer questions about how the contact forces are affected during breakage.

While already capable of making good predictions on granular breakage, this method can certainly be improved. For example, three simple breakage criteria were used in this paper. A breakage criterion where the breakage stress is based on a field of intraparticle stress may be more realistic for many materials. Also improvements in fracture

surface shape could greatly improve the accuracy at the granular level. This could be done either with calculating a stress distribution or by using the data from tomography to have a data based method for fracture surface generation. For possibly a more simple addition, adding available extensions to this method to model more breakage types, such as chipping, may increase accuracy of the method even further as well.

Declaration of competing interest

The authors declare that they have no known competing financial interests or personal relationships that could have appeared to influence the work reported in this paper.

Acknowledgment

This work was supported by a NASA Space Technology Research Fellowship, Grant No. 80NSSC19K1160.

Appendix. Calculating material properties for particles

For the purposes of building new particles, here we present an explanation on how to determine the material properties using just the information from the discrete level set function. The three key material properties to compute are the mass, center of mass, and the moment of inertia.

First we define the smoothed Heaviside function, $H(\phi)$, as,

$$H(\phi) = \begin{cases} 0 & \phi < -\epsilon \\ \frac{1}{2}\left(1 + \frac{\phi}{\epsilon} + \frac{sin(\frac{\pi\phi}{\epsilon})}{\pi}\right) & -\epsilon \leq \phi < \epsilon \\ 1 & \epsilon \leq \phi \end{cases} \tag{24}$$

where ϵ is a smoothness parameter set to $\epsilon = 1.5$. Assuming the particle has uniform density, ρ, and unitary grid spacing, the mass can be computed in 3D as,

$$m = \rho \sum_{i=1}^{I} \sum_{j=1}^{J} \sum_{k=1}^{K} H(-\phi(x_i, y_j, z_k)) \tag{25}$$

and in 2D,

$$m = \rho \sum_{i=1}^{I} \sum_{j=1}^{J} H(-\phi(x_i, y_j)) \tag{26}$$

where I, J and K are the maximum grid dimensions in each direction. The center of mass can then be computed in 3D,

$$\begin{aligned} \bar{x} &= \frac{\rho}{m} \sum_{i=1}^{I} \sum_{j=1}^{J} \sum_{k=1}^{K} H(-\phi(x_i, y_j, z_k)) x_i \\ \bar{y} &= \frac{\rho}{m} \sum_{i=1}^{I} \sum_{j=1}^{J} \sum_{k=1}^{K} H(-\phi(x_i, y_j, z_k)) y_j \\ \bar{z} &= \frac{\rho}{m} \sum_{i=1}^{I} \sum_{j=1}^{J} \sum_{k=1}^{K} H(-\phi(x_i, y_j, z_k)) z_k \end{aligned} \tag{27}$$

and in 2D,

$$\begin{aligned} \bar{x} &= \frac{\rho}{m} \sum_{i=1}^{I} \sum_{j=1}^{J} H(-\phi(x_i, y_j)) x_i \\ \bar{y} &= \frac{\rho}{m} \sum_{i=1}^{I} \sum_{j=1}^{J} H(-\phi(x_i, y_j)) y_j \end{aligned} \tag{28}$$

Then finally the moment of inertia for 3D,

$$I_{xx} = \rho \sum_{i=1}^{I} \sum_{j=1}^{J} \sum_{k=1}^{K} H(-\phi(x_i, y_j, z_k))[(y_j - \bar{y})^2 + (z_k - \bar{z})^2]$$

$$I_{yy} = \rho \sum_{i=1}^{I} \sum_{j=1}^{J} \sum_{k=1}^{K} H(-\phi(x_i, y_j, z_k))[(x_i - \bar{x})^2 + (z_k - \bar{z})^2]$$

$$I_{zz} = \rho \sum_{i=1}^{I} \sum_{j=1}^{J} \sum_{k=1}^{K} H(-\phi(x_i, y_j, z_k))[(x_i - \bar{x})^2 + (y_j - \bar{y})^2]$$

$$I_{yz} = I_{zy} = -\rho \sum_{i=1}^{I} \sum_{j=1}^{J} \sum_{k=1}^{K} H(-\phi(x_i, y_j, z_k))(y_j - \bar{y})(z_k - \bar{z})$$

$$I_{xz} = I_{zx} = -\rho \sum_{i=1}^{I} \sum_{j=1}^{J} \sum_{k=1}^{K} H(-\phi(x_i, y_j, z_k))(x_i - \bar{x})(z_k - \bar{z})$$

$$I_{xy} = I_{yx} = -\rho \sum_{i=1}^{I} \sum_{j=1}^{J} \sum_{k=1}^{K} H(-\phi(x_i, y_j, z_k))(x_i - \bar{x})(y_j - \bar{y}) \tag{29}$$

and in 2D,

$$I = \rho \sum_{i=1}^{I} \sum_{j=1}^{J} H(-\phi(x_i, y_j, z_k))[(x_i - \bar{x})^2 + (y_j - \bar{y})^2] \tag{30}$$

References

[1] N.H. Minh, Y.P. Cheng, A DEM investigation of the effect of particle-size distribution on one-dimensional compression, Géotechnique 63 (1) (2013) 44–53.

[2] R.D. Holtz, W.D. Kovacs, An Introduction to Geotechnical Engineering, in: Prentice-Hall Civil Engineering and Engineering Mechanics Series, Prentice-Hall, 1981.

[3] Andrea Billi, Grain size distribution and thickness of breccia and gouge zones from thin (<1m) strike-slip fault cores in limestone, J. Struct. Geol. 27 (10) (2005) 1823–1837.

[4] Itai Einav, Breakage mechanics - part 1: Theory, J. Mech. Phys. Solids 55 (6) (2007) 1274–1297.

[5] A.M. Evans, Ore Geology and Industrial Minerals: An Introduction, in: Geoscience Texts, Wiley, 1993.

[6] Oleg A. Sapozhnikov, Adam D. Maxwell, Brian MacConaghy, Michael R. Bailey, A mechanistic analysis of stone fracture in lithotripsy, J. Acoust. Soc. Am. 121 (2) (2007) 1190–1202.

[7] P.A. Cundall, O.D.L. Strack, A discrete numerical model for granular assemblies, Géotechnique 29 (1) (1979) 47–65.

[8] M.B. Cil, K.A. Alshibli, 3D Evolution of sand fracture under 1d compression, Géotechnique 64 (5) (2014) 351–364.

[9] Y.P. Cheng, Y. Nakata, M.D. Bolton, Discrete element simulation of crushable soil, Géotechnique 53 (7) (2003) 633–641.

[10] Pei Wang, Chloé Arson, Discrete element modeling of shielding and size effects during single particle crushing, Comput. Geotech. 78 (2016) 227–236.

[11] Jianfeng Wang, Haibin Yan, On the role of particle breakage in the shear failure behavior of granular soils by DEM, Int. J. Numer. Anal. Methods Geomech. 37 (8) (2013) 832–854.

[12] D.O. Potyondy, P.A. Cundall, A bonded-particle model for rock, Int. J. Rock Mech. Min. Sci. 41 (8) (2004) 1329–1364, Rock Mechanics Results from the Underground Research Laboratory, Canada.

[13] Oded Ben-Nun, Itai Einav, The role of self-organization during confined comminution of granular materials, Philos. Trans. R. Soc. Lond. A: Math. Phys. Eng. Sci. 368 (1910) (2010) 231–247.

[14] G.R. McDowell, J.P. de Bono, On the micro mechanics of one-dimensional normal compression, Géotechnique 63 (11) (2013) 895–908.

[15] Reid Kawamoto, José Andrade, Takashi Matsushima, A 3-d mechanics-based particle shape index for granular materials, Mech. Res. Commun. 92 (2018) 67–73.

[16] Wadi H. Imseeh, Khalid A. Alshibli, 3D Finite element modelling of force transmission and particle fracture of sand, Comput. Geotech. 94 (2018) 184–195.

[17] Pavel Iliev, Falk Wittel, Hans J. Herrmann, Evolution of fragment size distributions from the crushing of granular materials, Phys. Rev. E 99 (2019).

[18] Alexander Potapov, Charles Campbell, A three-dimensional simulation of brittle solid fracture, Internat. J. Modern Phys. C 7 (1996) 717–729.

[19] John A Herbst, Alexander V Potapov, Making a discrete grain breakage model practical for comminution equipment performance simulation, Powder Technol. 143–144 (2004) 144–150.

[20] Narcés Jiménez-Herrera, Gabriel K.P. Barrios, Luí s Marcelo Tavares, Comparison of breakage models in DEM in simulating impact on particle beds, Adv. Powder Technol. 29 (3) (2018) 692–706.

[21] Fan Zhu, Jidong Zhao, Modeling continuous grain crushing in granular media: A hybrid peridynamics and physics engine approach, Comput. Methods Appl. Mech. Engrg. 348 (2019) 334–355.
[22] Guilhem Mollon, Jidong Zhao, 3D Generation of realistic granular samples based on random fields theory and fourier shape descriptors, Comput. Methods Appl. Mech. Engrg. 279 (2014) 46–65.
[23] Reid Kawamoto, Edward Andò, Gioacchino Viggiani, José E. Andrade, Level set discrete element method for three-dimensional computations with triaxial case study, J. Mech. Phys. Solids 91 (2016) 1–13.
[24] Ivan Vlahinić, Edward Andò, Gioacchino Viggiani, José E. Andrade, Towards a more accurate characterization of granular media: extracting quantitative descriptors from tomographic images, Granul. Matter 16 (1) (2014) 9–21.
[25] Reid Kawamoto, Edward Ando, Gioacchino Viggiani, Jose E. Andrade, All you need is shape: Predicting shear banding in sand with LS-DEM, J. Mech. Phys. Solids 111 (2018) 375–392.
[26] Kenneth Langstreth Johnson, Kenneth Langstreth Johnson, Contact Mechanics, Cambridge university press, 1987.
[27] M. Jean, The non-smooth contact dynamics method, Comput. Methods Appl. Mech. Engrg. 177 (3) (1999) 235–257.
[28] O.R. Walton, R.L. Braun, Simulation of rotary-drum and repose tests for frictional spheres and rigid sphere clusters, in: joint Department of Energy/National Science Foundation (DOE/NSF) workshop on flow of particulates, 1993.
[29] Keng-Wit Lim, José E. Andrade, Granular element method for three-dimensional discrete element calculations, Int. J. Numer. Anal. Methods Geomech. 38 (2) (2014) 167–188.
[30] W. Weibull, A Statistical Theory of the Strength of Materials, in: Handlingar / Ingeniörsvetenskapsakademien, Generalstabens litografiska anstalts förlag, 1939.
[31] G.R. McDowell, On the yielding and plastic compression of sand, Soils Found. 42 (1) (2002) 139–145.
[32] A F.L. Nakata, M Hyde, H Hyodo, Murata, A probabilistic approach to sand particle crushing in the triaxial test, Geotechnique 49 (1999) 567–583.
[33] Yupeng Jiang, Hans J. Herrmann, Fernando Alonso-Marroquin, A boundary-spheropolygon element method for modelling sub-particle stress and particle breakage, Comput. Geotech. 113 (2019) 103087.
[34] Mark Sussman, Peter Smereka, Stanley Osher, A level set approach for computing solutions to incompressible two-phase flow, J. Comput. Phys. 114 (1) (1994) 146–159.
[35] M.B. Cil, K.A. Alshibli, 3D Assessment of fracture of sand particles using discrete element method, Géotech. Lett. 2 (3) (2012) 161–166.
[36] R.C. Hurley, J. Lind, D.C. Pagan, M.C. Akin, E.B. Herbold, In situ grain fracture mechanics during uniaxial compaction of granular solids, J. Mech. Phys. Solids 112 (2018) 273–290.
[37] N.S. Weerasekara, M.S. Powell, P.W. Cleary, L.M. Tavares, M. Evertsson, R.D. Morrison, J. Quist, R.M. Carvalho, The contribution of DEM to the science of comminution, Powder Technol. 248 (2013) 3–24, Discrete Element Modelling.
[38] Marcus Johansson, Magnus Bengtsson, Magnus Evertsson, Erik Hulthén, A fundamental model of an industrial-scale jaw crusher, Miner. Eng. 105 (2017) 69–78.
[39] J. Atkinson, The Mechanics of Soils and Foundations, second ed., in: Spon Text, Taylor & Francis, 2007.
[40] Yukio Nakata, Masayuki Hyodo, Adrian F.L. Hyde, Yoshinori Kato, Hidekazu Murata, Microscopic particle crushing of sand subjected to high pressure one-dimensional compression, Soils Found. 41 (1) (2001) 69–82.
[41] Zhijie Wang, Axel Ruiken, Felix Jacobs, Martin Ziegler, A new suggestion for determining 2d porosities in DEM studies, Geomech. Eng. 7 (2014) 665–678.
[42] Armando Coco, Giovanni Russo, Finite-difference ghost-point multigrid methods on Cartesian grids for elliptic problems in arbitrary domains, J. Comput. Phys. 241 (2013) 464–501.
[43] Hakon Wadell, Volume, shape, and roundness of rock particles, J. Geol. 40 (5) (1932) 443–451.
[44] Tabassom Afshar, Mahdi Disfani, Guillermo Narsilio, Arul Arulrajah, Changes to grain properties due to breakage in a sand assembly using synchrotron tomography, EPJ Web Conf. 140 (2017) 07004.
[45] F.N. Altuhafi, M.R. Coop, Changes to particle characteristics associated with the compression of sands, Géotechnique 61 (6) (2011) 459–471.
[46] Y. Sun, B. Indraratna, S. Nimbalkar, Three-dimensional characterisation of particle size and shape for ballast, Géotech. Lett. 4 (3) (2014) 197–202.
[47] B. Zhao, J. Wang, M.R. Coop, G. Viggiani, M. JIANG, An investigation of single sand particle fracture using x-ray micro-tomography, Géotechnique 65 (8) (2015) 625–641.
[48] Masataka Takei, Osamu Kusakabe, Taketo Hayashi, Time-dependent behavior of crushable materials in one-dimensional compression tests, Soils Found. 41 (1) (2001) 97–121.
[49] Zeynep Karatza, Edward Andò, Stefanos-Aldo Papanicolopulos, Gioacchino Viggiani, Jin Y. Ooi, Effect of particle morphology and contacts on particle breakage in a granular assembly studied using x-ray tomography, Granul. Matter 21 (3) (2019) 44.